colloids and interfaces

MDPI

Article

Application of Bio-Based Wrinkled Surfaces as Cell Culture Scaffolds

Hironori Izawa [1,*], Noriko Okuda [1], Tomoe Yonemura [1], Kohei Kuroda [2], Kosuke Ochi [2], Shinsuke Ifuku [1], Minoru Morimoto [3], Hiroyuki Saimoto [1], Mayuko Noda [2], Kazuo Azuma [2,*], Yoshiharu Okamoto [2] and Norihiko Ito [2,*]

1 Graduate School of Engineering, Tottori University, 4-101 Koyama-Minami, Tottori 680-8550, Japan; i084nkys1@yahoo.co.jp (N.O.); tyairo24@gmail.com (T.Y.); sifuku@chem.tottori-u.ac.jp (S.I.); saimoto@chem.tottori-u.ac.jp (H.S.)

2 Department of Veterinary Clinical Medicine, Tottori University, 4-101 Koyama-Minami, Tottori 680-8550, Japan; nanararayu@gmail.com (K.K.); kosukeochi28@gmail.com (K.O.); noda-m@adm.tottori-u.ac.jp (M.N.); yokamoto@muses.tottori-u.ac.jp (Y.O.)

3 Division of Instrumental Analysis, Research Center for Bioscience and Technology, Tottori University, Tottori 680-8550, Japan; morimoto@chem.tottori-u.ac.jp

* Correspondence: h-izawa@chem.tottori-u.ac.jp (H.I.); kazu-azuma@muses.tottori-u.ac.jp (K.A.); taromobile@me.com (N.I.); Tel.: +81-857-31-5813 (H.I.); +81-857-31-5433 (K.A.); +81-857-31-6058 (N.I.)

Received: 2 March 2018; Accepted: 23 March 2018; Published: 26 March 2018

Abstract: Microscopic surface architectures that can be easily manufactured have been in demand as mechano-structural cues for tissue engineering. Microscopic surface reliefs synthesized by wrinkling were expected as cell culture scaffolds for cell proliferation, control of cellular alignment and differentiation, and spheroid generation. We previously developed bio-based wrinkled films prepared via lignification-mimetic reactions and drying. Although these films are expected as a candidate for cell culture scaffolds, stability and morphology of the wrinkled surfaces in aqueous buffer solutions were not explored. Here, we investigate the surface morphologies of the wrinkled films in phosphate-buffered saline, and their application to 3T3 cell culture. The wrinkled film prepared with the immersion treatment at 40 °C maintained its wrinkled structure in phosphate-buffered saline even after five days, although the wrinkles were broadened by hydration of the skin layer. Interestingly, higher cell numbers were observed in the 3T3 cell culture using the wrinkled film than using flat film with the same surface composition. In addition, the high biocompatibility of the wrinkled film was confirmed by in vivo experiments. These results strongly encourage application of the wrinkled film as a mechano-structural cue. Studies of the advanced applications for the wrinkled films are now in progress.

Keywords: chitosan; surface wrinkling; skin layer; horseradish peroxidase; cell culture substrate; 3T3 cell

1. Introduction

Tissue engineering has attracted attention as a therapeutic method for replacing damaged tissues and organs [1,2]. Development of scaffold materials that can modulate the proliferation, self-renewal, and differentiation of multipotent stem cells into different lineages is a key aspect of tissue engineering [3]. Extensive research has revealed that mechano-structural cues, such as elasticity and topography differentially modulate cell fate in a hierarchical response [4]. Thus, technologies for easy fabrication of microscopic surface architecture would contribute to progress in tissue engineering.

Surface wrinkling is a physical process that creates unique topographies in nature [5,6]. Nano/microscopic surface reliefs synthesized by wrinkling have been used for nano/microscopic

wrinkled surfaces in optical [7] and electronic devices [8], surface-enhanced Raman spectroscopy substrates [9], the realization of tunable wettability [10], and adhesion [11], and cell culture scaffolds [12–17]. In the application for cell culture scaffolds, wrinkled surfaces with unique topographies have been used for cell proliferation [12], control of cellular alignment and differentiation [13,14,16], and spheroid generation [15,17].

Recently, we reported an original approach to surface wrinkling [18–21]. In this method, a skin layer is synthesized on a chitosan (CS) film via immersion in a methanol solution containing a phenolic acid and subsequent surface reaction by horseradish peroxidase (HRP) mimicking wood lignification. We revealed that the immersion process induced surface wrinkling by the formation of covalent bonds between the CS substrate and phenolic acid. The phenolic acid-bound moieties acted as reaction sites for crosslinking via the HRP-catalyzed reaction and yielded a skin layer on the submicron order. The crosslinking structure capable of skin formation consisted of ionic bonds composed of CS and oligomeric phenolic acid residues on CS [18]. A surface relief with micron-scale wrinkles is formed upon drying as a result of inhomogeneous shrinkage (Figure 1). This is a totally bio-based system involving green materials and processes. In addition, we found that the wrinkled surfaces maintained their structure in water [19]. Although this result encouraged us to apply the wrinkled surfaces for use as a cell culture scaffold, stability, and morphology of the wrinkled films in aqueous buffer solutions were not explored. In addition, the wrinkled films are potential biomaterials because CS, their main constituent, has high biocompatibility [22]. However, the toxicity of oligophenolic acid residues present around film surface is concerned. Therefore, biocompatibility of the wrinkled films should be explored.

Here, we investigate a detailed characterization of the wrinkled surfaces in phosphate-buffered saline (PBS) by atomic force microscopy (AFM) analysis, and the 3T3 cell culture on the wrinkled surfaces, in order to confirm the potential applicability of these synthesized surfaces as mechano-structural cues. In addition, we investigate the biocompatibility of the wrinkled films by implant placement in mice.

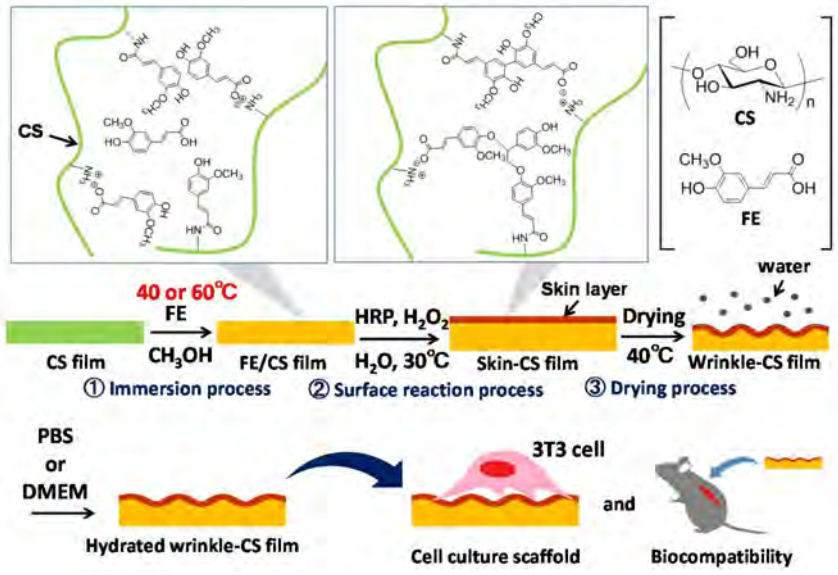

Figure 1. Schema of this study.

2. Results and Discussion

2.1. AFM Analysis of the Wrinkle-CS Films in Air and PBS

The wrinkle-CS films were prepared via immersion in a methanol solution containing ferulic acid (FE) at 40 °C and 60 °C, the HRP-catalysed surface reaction, and drying in accordance

with our previous report (Figure 1) [20]. Figure 2a–c show AFM images of the wrinkle-CS films prepared via immersion treatments at 40 °C and 60 °C, and the original CS film under atmospheric conditions, respectively. Figure 2d shows a detailed characterization of the wrinkles. Wrinkling under treatments at 40 °C and 60 °C was similar to that in our previous reports [20]: the mean wrinkle wavelengths and amplitudes at 40 °C were 2.09 ± 0.45 and 1.28 ± 0.16 μm, and those at 60 °C were 0.73 ± 0.18 and 0.44 ± 0.06 μm, respectively. Roughness measures were 331 and 101 nm, respectively. Interestingly, semi-spherical bumps of ca. 100 nm were observed on both magnified images. This micro-structure was not observed in our previous analysis with SEM. These were presumably generated by the strong aggregation of CS and an oligomeric FE side chain. The Young's moduli of the wrinkled surfaces estimated by force-curve measurements were 4.81 ± 1.7 and 2.80 ± 0.34 GPa for the 40 °C and 60 °C immersion treatments, respectively. This result is consistent with our previous report [21]. In this wrinkling system, CS around the film surface was degraded in the immersion process, which was accelerated at higher immersion temperature, and the degradation in turn caused smaller wrinkles.

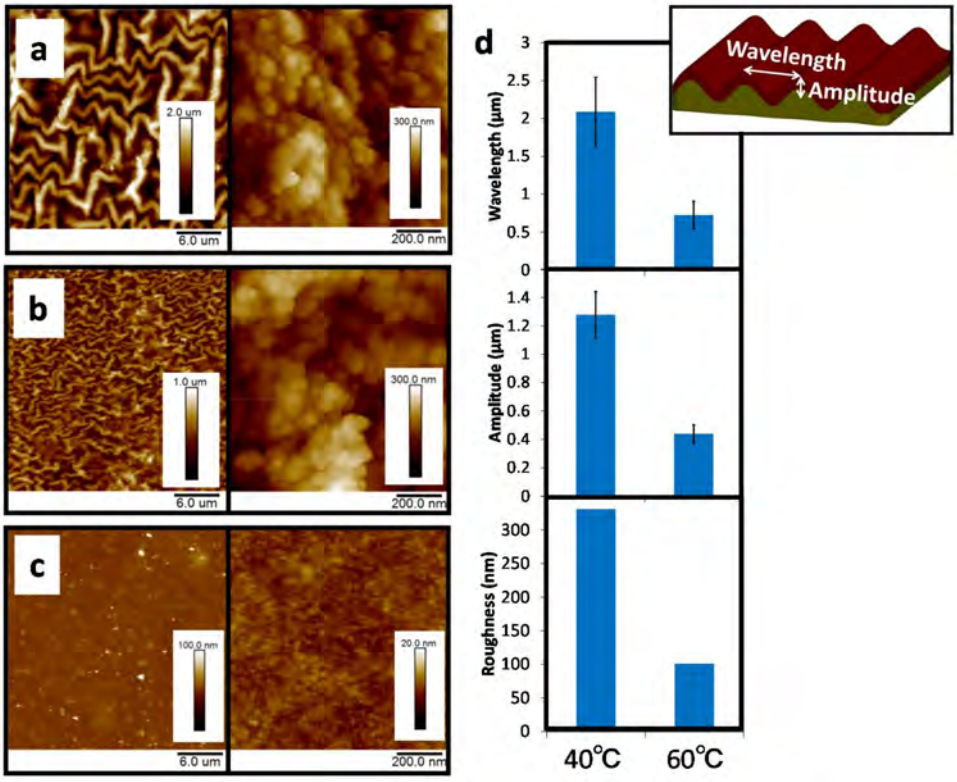

Figure 2. AFM images of the wrinkle-CS films prepared via immersion treatment at 40 °C (**a**) and 60 °C (**b**); and the original CS film (**c**) under atmospheric conditions and detailed characterization of the wrinkles (**d**). Error bars reflect the standard deviations.

In order to evaluate the wrinkle morphology after water swelling, the films were soaked in PBS (pH 7.4) for five days at 37 °C and then subjected to AFM analysis. Figure 3a–c show AFM images of the wrinkle-CS films prepared via immersion treatments at 40 °C and 60 °C, and the original CS film under the PBS, respectively. Detailed characterization of wrinkles is shown in Figure 3d. If the skin layer had returned to the same hydration state as the skin-CS film, the wrinkles would have completely disappeared (Figure 4a). However, the wrinkled surface prepared via the immersion treatment at 40 °C was preserved after hydration. Its mean wrinkle wavelength and amplitude were 3.03 ± 0.31 and 0.56 ± 0.05 μm, respectively. Wavelength was increased but amplitude was decreased compared to before hydration. In addition, roughness decreased to 121 nm. These results

indicate the wrinkles were spread out by hydration of the skin layer, but the hydration stopped before completion (Figure 4b). Interestingly, the semi-spherical bumps of ca. 100 nm were preserved even after swelling. In the wrinkle-CS films prepared via immersion treatment at 60 °C, wrinkles disappeared due to the high hydration of the skin layer, in which roughness was decreased to 31 nm. As already mentioned, immersion treatment at higher temperature accelerated decomposition of CS around the film surface [21], and in turn caused decreased crystallinity of CS [23]. Therefore, the skin layer composed of a lower molecular weight of CS allowed higher hydration. Interestingly, however, the semi-spherical bumps could still be observed. In addition, a slight dissipative pattern appeared on the surface. This was probably a remnant of the surface wrinkling remaining on the skin layer (Figure 4c). The mean wavelength and amplitude of the remnant pattern were 1.43 ± 0.40 and 0.10 ± 0.03 μm, respectively. Young's modulus of the surfaces via the immersion treatment at 40 °C was 6.01 ± 0.14 MPa.

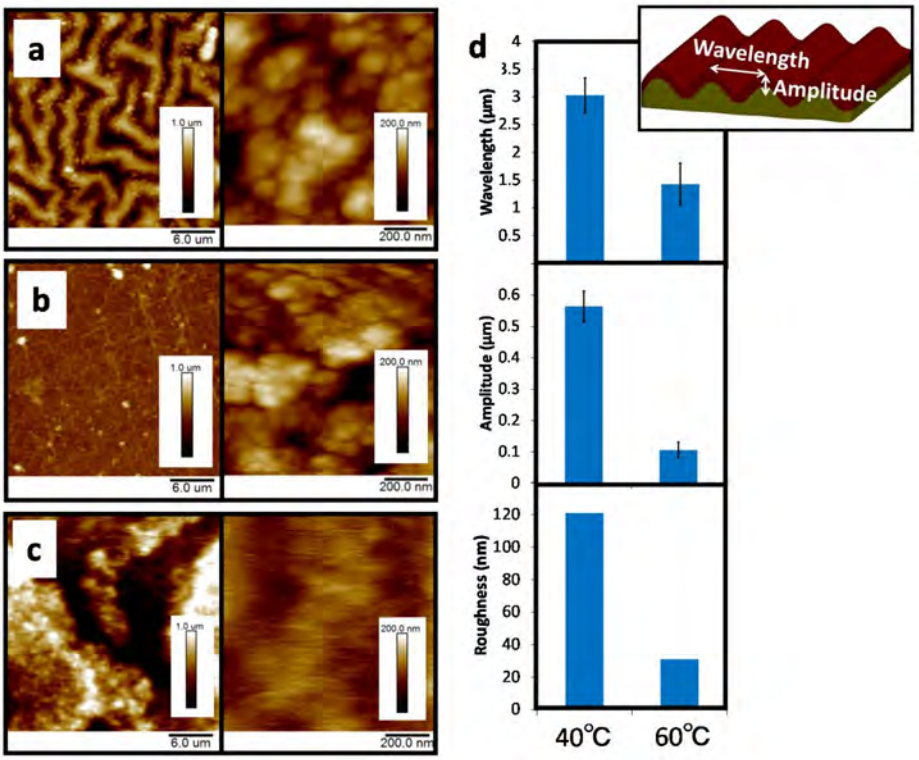

Figure 3. AFM images of the wrinkle-CS films prepared via immersion treatment at 40 °C (**a**) and 60 °C (**b**); and the original CS film (**c**) under PBS and detailed characterization of the wrinkles (**d**). Error bars reflect the standard deviations.

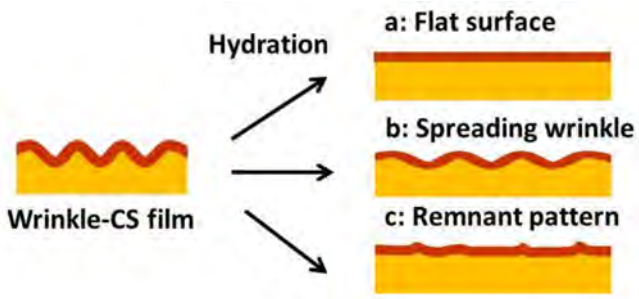

Figure 4. Illustration of the hydrated CS film assuming the skin layer completely hydrates (**a**) and the observed hydration behaviour on the wrinkle-CS films prepared via immersion treatment at 40 °C (**b**) and 60 °C (**c**).

2.2. 3T3 Cell Culture on the Wrinkle-CS Film

In order to evaluate the effects of the wrinkled surface composed of the ionic crosslinking of CS and oligomeric FE side chains on cellular behaviour, 3T3 cells were cultured on the wrinkle-CS film prepared via the immersion treatment at 40 °C. The cell culture was carried out with DMEM. Figure 5a–d show optical microscopy images of the 3T3 cells adhered to the respective substrates after two days. In the wrinkle-CS film and polystyrene plate, the 3T3 cells were near confluent. Cell counts and frequencies of dead cell are shown in Figure 5e. For the wrinkle-CS film, cell numbers and the frequency of dead cells were $3.20 \pm 0.87 \times 10^5$ mL^{-1} and $20.8 \pm 4.8\%$, respectively; these were higher and lower, respectively, than those of the skin-CS film with a flat surface, indicating the wrinkle morphology had some positive effects. The introduction of specific subcellular scaled surface features often promotes cell adhesion. The enhanced cell attachment of 3T3 cells on wrinkled surfaces having similar size and morphology was reported [14,24]. Thus, promotion of cell attachment by wrinkles is considered one reason for the higher cell number. Interestingly, the cell numbers and frequencies of dead cells for the wrinkle-CS film/skin-CS film were much higher and lower, respectively, than those of the CS film. This result clearly indicates that the skin layer composed of the ionic crosslinking of CS and oligomeric FE side chains has higher compatibility to 3T3 cells than the CS film surface. In the control polystyrene plate (cell culture dish), the cell number and frequency of dead cells were $2.82 \pm 0.68 \times 10^5$ mL^{-1} and $21.1 \pm 9.4\%$, respectively, which were comparable to those of the wrinkle-CS film. Generally, the polystyrene plate efficiently proliferate the 3T3 cells. Thus, this result indicates the wrinkle-CS film is suitable as a cell culture substrate.

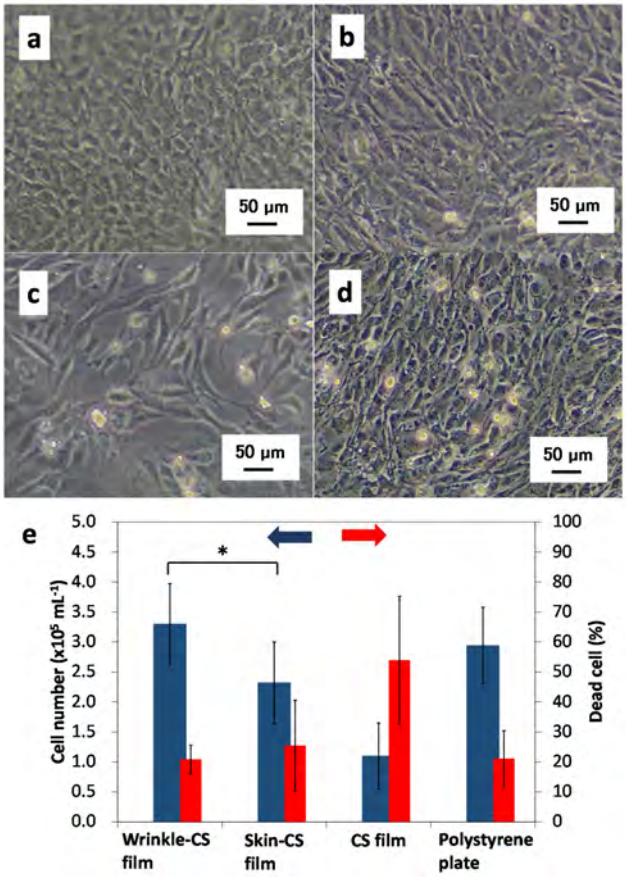

Figure 5. Optical microscopy images of 3T3 cells adhered on the wrinkle-CS film (40 °C) (**a**); the skin-CS film (Un-dried film after surface reaction process as shown in Figure 1) (**b**); the CS film (**c**); and the polystyrene plate (cell culture dish) (**d**). Analytical results of cell number and dead cells (**e**). Error bars reflect the standard deviations ($n = 10$, * $p < 0.05$).

2.3. 3T3 Biocompatibility of the Wrinkle-CS Film

Figure 6a shows a schematic illustration of the in vivo evaluation. The results of histopathological evaluations of animals of the wrinkle-CS film, skin-CS film, and negative control are presented in Figure 6b–g. In the wrinkle-CS film, many neutrophils, fibroblasts, and collagens were observed. In the skin-CS film, many fibroblast and collagens were also observed. On the other hand, there are a few neutrophils in the skin-CS film. In the negative control, there are a few neutrophils, fibroblasts, and collagens. The infiltrations of neutrophils (inducing inflammation) is one of first actions in various biological events such as wound healing process [25,26]. In chitin and chitosan scaffolds, the three-dimensional (3D) structure is very effective for inducing and proliferations of cells [27]. On the other hand, there are a few neutrophils in the skin-CS film. These results indicate that the 3D structure of the wrinkle-CS films induce neutrophils to the films. In the wound healing process, migration periods after inflammation are also important [28]. The migrations of fibroblasts were observed in the wrinkle-CS and skin-CS film. CS has high migration activities in vivo [26]. The results of the present study indicate that the wrinkle-CS film induces neutrophil infiltration and the migration of fibroblasts, which might indicate that the wrinkle-CS films are effective in enhancing wound healing processes. Further study with an experimental model of wound healing must be performed.

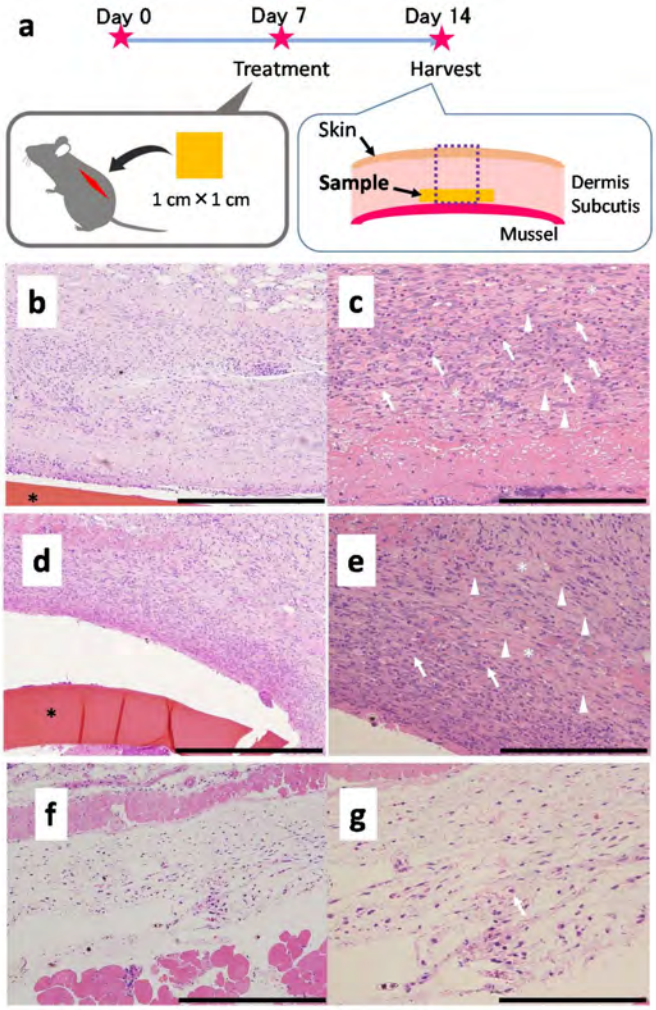

Figure 6. Evaluation of biocompatibility. Schema of the animal experiment (**a**); Histopathological properties of the wrinkle-CS film (**b**,**c**) and the skin-CS film (**d**,**e**); and negative control (**f**,**g**) on day 7. Scale bars are 400 μm (**b**,**d**,**f**) and 200 μm (**c**,**e**,**g**). The black asterisks indicate films. The arrows indicate the neutrophils, the arrow heads indicate fibroblasts and white asterisks indicate collagens in each field.

3. Conclusions

Surface morphologies of bio-based wrinkled films, prepared via the HRP-catalyzed surface reaction of FE and drying in PBS were investigated by AFM analysis. The wrinkled film with immersion treatment at 40 °C maintained the wrinkles even after five days. This wrinkled film showed good performance as a cell culture substrate for 3T3 cells, which was comparable to the performance of the polystyrene plate. This result strongly encourages application of the wrinkled film as a mechano-structural cue. Moreover, the wrinkled film showed good biocompatibility in an in vivo experiment with mice. Potential application for wound healing was suggested. Studies of these advanced applications for the wrinkled films are now in progress.

4. Materials and Methods

4.1. Materials

CS with an un-deacetylated 23.5% fraction (elemental analysis) (M_n: 5.6 × 10^4; M_w/M_n: 2.36; GPC analysis with Pullulan standards) was supplied by Koyo Chemical (Tottori, Japan). FE was purchased from Tokyo Chemical Industry (Tokyo, Japan). HRP (274 U/mg) was purchased from Toyobo (Osaka, Japan). PBS (PH 7.4, 10×; Gibco^{TM}), penicillin-streptomycin-neomycin (PSN) antibiotic mixture (Gibco^{TM}), Dulbecco's modified Eagle medium, high glucose (DMEM) (Gibco^{TM}), and Trypan blue (Gibco^{TM}) were purchased from Thermo Fisher Scientific (Waltham, MA, USA). Finally, 0.25 *w*/*v*% Trypsin-1 mmol/L EDTA·4Na solution with phenol red was purchased from Wako Pure Chemical Industries (Osaka, Japan). Other reagents used were commercial grade and used without further purification.

4.2. Instrumentation

AFM images and force curves were measured by a MultiMode 8 with NanoScope V controller (Bruker, Santa Barbara, CA, USA). Details on the measurements are given below. M_n and M_w/M_n of CS were measured by gel permutation chromatography (GPC) at 40 °C in acetate buffer solution eluent: Asahipak GS-220 HQ, Asahipak GS-320 HQ, Asahipak GS-520 HQ, and Asahipak GS-2G 7B (Shodex, Tokyo, Japan), an L-2130 pump, and an RI-detector L-2490 (Hitachi, Tokyo, Japan). The flow rate was 0.5 mL/min.

4.3. Preparation of the CS Film

CS (2.0 g) was dissolved in 100 mL of an acidic aqueous solution containing 0.5-mL acetic acid. Then, 10 mL of the CS solution was added to a Teflon Petri dish (ϕ = 50 mm) and degassed under reduced pressure. The CS solution was heated at 50 °C for 24 h to yield a CS film after evaporation. The film was then heated at 50 °C under reduced pressure for 12 h. The inhomogeneous edge of the film was cut down with scissors. The weight and thickness of the CS film were ca. 0.15 g and ca. 100 μm, respectively.

4.4. Surface Wrinkling of Films

A CS film was immersed in 20-mL methanol containing 0.05-g/mL FE at 40 °C or 60 °C for 24 h. The resulting film was removed and soaked in 10 mL of water, followed by the prompt addition of the HRP (1 mL, 137 U) and H_2O_2 (200 μL, 30% concentration). The system was kept at 30 °C for 12 h, after which the film was removed and dried at 40 °C for 12 h.

4.5. AFM and Force Curve Measurement

For the observation of the films, samples cut into 5-mm squares were attached to a steel plate with a diameter of 12 mm using double-sided tape, which were then set on the AFM sample stage. AFM images were obtained in PeakForce Tapping mode on a MultiMode 8 at room temperature.

We used two different types of cantilever tips: an NCHV-A (spring constant: 40 N/m; from Bruker) for the observations in air; and a ScanAsystFluid (spring constant: 0.7 N/m; from Bruker Corp.) for observations in PBS. The images were captured in 256 × 256 data points for a 1 μm × 1 μm, 10 μm × 10 μm (image data not shown), or 30 μm × 30 μm scan area with a scan rate of 0.5–1.8 Hz. The surface features were analysed using the image data from the 10 μm × 10 μm scan area. Surface roughness was determined using the software bundled with NanoScope, and amplitude was calculated by the difference between the peak and valley in the sectional view, while the wavelength was determined as the distance of between parallel "mountains", which can be observed in the top view.

For force-curve analysis, the spring constants of the cantilevers were calibrated by the thermal tune method [29]. In order to estimate the moduli, 10 force curves were acquired for each sample at the top of the mountain. The maximum loading forces were 200 nN in air and 50 nN in PBS. For the force-curve analysis, the Hertzian model [30] was used to calculate the Young's modulus by the software bundled with NanoScope. The Hertzian model is expressed as $F = 4E\sqrt{R}\delta^{3/2}/3(1-\nu^2)$, where F is the loading force, E is the Young's modulus to be determined, R is the tip radius, ν is the Poisson's ratio, and δ is the indentation depth. In the numerical calculations, the probing-tip radii were postulated to be 10 nm for the observations in air and 18 nm for PBS, while the Poisson's ratios were assumed to be 0.3 in the case of air and 0.45 in the case of PBS [31].

4.6. In Vitro Cell Culture

The wrinkle-CS films (diameter: 14 mm) for the in vitro study were sterilized by immersion in PBS (50 mL) containing a PSN antibiotic mixture (0.5 mL). These films were set on the bottoms of the 24-well culture plates (FALCON®, Corning, NY, USA). Each film was fixed by a silicon ring (outside diameter: 16 mm; inside diameter: 13 mm); 0.5 mL of 3T3 cell solution (3.8×10^4 cells/mL 3T3 cells diluted by DMEM) was seeded and cultured for two days (37 °C, 5% CO_2). After incubation, the cells were washed twice with 0.5 mL PBS, and then peeled by trypsin. The peeled cells (10 μL) were mixed with trypan blue (10 μL). The numbers of the cells were calculated by a haemocytometer with an optical microscope.

4.7. Animals

C57BL/6 mice (six-week-old females) were purchased from CLEA Japan (Osaka, Japan). All mice were maintained under conventional conditions. The Animal Research Committee of Tottori University approved of the care and use of mice in this study (permission no.: 15-T-40).

4.8. In Vivo Evaluation

In vivo evaluation was performed according to our previous method with slight modifications [32]. A schematic illustration of the in vivo test is shown in Figure 6a. On day 0, the posterior region of the animal was clipped and disinfected with 5% *w*/*v* chlorhexidine gluconate (Pfizer, New York, NY, USA) and 50% *w*/*v* isopropanol (Yoshida Pharmaceutical, Tokyo, Japan). Skin incisions (1.2-cm long) were made after inhalation of 2–3% isoflurane. In the control group (two mice), wounds were closed using a medical stapler (Johnson and Johnson, Tokyo, Japan). For the wrinkle-CS group, the film (1.0 × 1.0 cm) was applied to the subcutaneous layer and the wounds were then closed with a medical stapler.

Skin and subcutaneous tissue samples were obtained on day 7, from mice anesthetized via the inhalation of 5% isoflurane. The samples obtained included the surrounding epidermis, subcutaneous tissues, and muscle layers around the films. The tissues were fixed in 10% buffered formalin.

Thin sections (4 μm) were prepared from each sample for histological observation after hematoxylin-eosin (HE) staining. Each section was examined microscopically.

Acknowledgments: This work was supported in part by JSPS KAKENHI grant number 16K05916.

Author Contributions: H.I. and N.I. conceived the experiment. H.I. and K.A. wrote paper. N.O., T.Y., K.K., K.O., and M.N. performed experiments. K.A. and N.O. performed in animal experiments. H.I, S.I., M.M., H.S., K.A., Y.O. and N.I. directed the research.

Conflicts of Interest: There are no conflicts of interest to declare.

Abbreviations

CS	Chitosan
HRP	Horseradish peroxidase
PBS	Phosphate buffered saline
AFM	Atomic force microscopy
FE	Ferulic acid

References

1. Drury, J.L.; Mooney, D.J. Hydrogels for tissue engineering: Scaffold design variables and applications. *Biomaterials* **2003**, *24*, 4337–4351. [CrossRef]
2. Lutolf, M.P.; Hubbell, J.A. Synthetic biomaterials as instructive extracellular microenvironments for morphogenesis in tissue engineering. *Nat. Biotechnol.* **2005**, *23*, 47–55. [CrossRef] [PubMed]
3. Metavarayuth, K.; Sitasuwan, P.; Zhao, X.; Lin, Y.; Wang, Q. Influence of Surface Topographical Cues on the Differentiation of Mesenchymal Stem Cells in Vitro. *ACS Biomater. Sci. Eng.* **2016**, *2*, 142–151. [CrossRef]
4. Uto, K.; Tsui, J.H.; DeForest, C.A.; Kim, D.H. Dynamically tunable cell culture platforms for tissue engineering and mechanobiology. *Prog. Polym. Sci.* **2017**, *65*, 53–82. [CrossRef] [PubMed]
5. Genzer, J.; Groenewold, J. Soft matter with hard skin: From skin wrinkles to templating and material characterization. *Soft Matter* **2006**, *2*, 310–323. [CrossRef]
6. Ionov, L. Biomimetic 3D self-assembling biomicroconstructs by spontaneous deformation of thin polymer films. *J. Mater. Chem.* **2012**, *22*, 19366–19375. [CrossRef]
7. Ohzono, T.; Suzuki, K.; Yamaguchi, T.; Fukuda, N. Tunable Optical Diffuser Based on Deformable Wrinkles. *Adv. Opt. Mater.* **2013**, *1*, 374–380. [CrossRef]
8. Lee, S.G.; Kim, H.; Choi, H.H.; Bong, H.; Park, Y.D.; Lee, W.H.; Cho, K. Evaporation-Induced Self-Alignment and Transfer of Semiconductor Nanowires by Wrinkled Elastomeric Templates. *Adv. Mater.* **2013**, *25*, 2162–2166. [CrossRef] [PubMed]
9. Stenberg, H.; Matikainen, A.; Daniel, S.; Nuutinen, T.; Stenberg, P.; Honkanen, S.; Pakkanen, T.; Vahimaa, P.; Suvanto, M. Self-organized Polymer Wrinkles: A Lithography-free Pathway for Surface-enhanced Raman Scattering (SERS) Substrates. *Macromol. Mater. Eng.* **2015**, *300*, 386–390. [CrossRef]
10. Li, Y.Y.; Dai, S.X.; John, J.; Carter, K.R. Superhydrophobic Surfaces from Hierarchically Structured Wrinkled Polymers. *ACS Appl. Mater. Interfaces* **2013**, *5*, 11066–11073. [CrossRef] [PubMed]
11. Davis, C.S.; Martina, D.; Creton, C.; Lindner, A.; Crosby, A.J. Enhanced Adhesion of Elastic Materials to Small-Scale Wrinkles. *Langmuir* **2012**, *28*, 14899–14908. [CrossRef] [PubMed]
12. Aufan, M.R.; Sumi, Y.; Kim, S.; Lee, J.Y. Facile Synthesis of Conductive Polypyrrole Wrinkle Topographies on Polydimethylsiloxane via a Swelling-Deswelling Process and Their Potential Uses in Tissue Engineering. *ACS Appl. Mater. Interfaces* **2015**, *7*, 23454–23463. [CrossRef] [PubMed]
13. Chen, A.; Lieu, D.K.; Freschauf, L.; Lew, V.; Sharma, H.; Wang, J.X.; Nguyen, D.; Karakikes, I.; Hajjar, R.J.; Gopinathan, A.; et al. Shrink-Film Configurable Multiscale Wrinkles for Functional Alignment of Human Embryonic Stem Cells and their Cardiac Derivatives. *Adv. Mater.* **2011**, *23*, 5785–5791. [CrossRef]
14. Greco, F.; Fujie, T.; Ricotti, L.; Taccola, S.; Mazzolai, B.; Mattoli, V. Microwrinkled Conducting Polymer Interface for Anisotropic Multicellular Alignment. *ACS Appl. Mater. Interfaces* **2013**, *5*, 573–584. [CrossRef] [PubMed]
15. Gu, J.J.; Li, X.Y.; Ma, H.C.; Guan, Y.; Zhang, Y.J. One-step synthesis of PHEMA hydrogel films capable of generating highly ordered wrinkling patterns. *Polymer* **2017**, *110*, 114–123. [CrossRef]
16. Guvendiren, M.; Burdick, J.A. The control of stem cell morphology and differentiation by hydrogel surface wrinkles. *Biomaterials* **2010**, *31*, 6511–6518. [CrossRef] [PubMed]

17. Zhao, Z.Q.; Gu, J.J.; Zhao, Y.N.; Guan, Y.; Zhu, X.X.; Zhang, Y.J. Hydrogel Thin Film with Swelling-Induced Wrinkling Patterns for High-Throughput Generation of Multicellular Spheroids. *Biomacromolecules* **2014**, *15*, 3306–3312. [CrossRef] [PubMed]
18. Izawa, H. Preparation of biobased wrinkled surfaces via lignification-mimetic reactions and drying: A new approach for developing surface wrinkling. *Polym. J.* **2017**, *49*, 759–765. [CrossRef]
19. Izawa, H.; Dote, Y.; Okuda, N.; Sumita, M.; Ifuku, S.; Morimoto, M.; Saimoto, H. Wood-mimetic skins prepared using horseradish peroxidase catalysis to induce surface wrinkling of chitosan film upon drying. *Carbohydr. Polym.* **2017**, *173*, 519–525. [CrossRef] [PubMed]
20. Izawa, H.; Okuda, N.; Ifuku, S.; Morimoto, M.; Saimoto, H.; Rojas, O.J. Bio-based Wrinkled Surfaces Harnessed from Biological Design Principles of Wood and Peroxidase Activity. *ChemSusChem* **2015**, *8*, 3892–3896. [CrossRef] [PubMed]
21. Izawa, H.; Okuda, N.; Moriyama, A.; Miyazaki, Y.; Ifuku, S.; Morimoto, M.; Saimoto, H. Biobased Wrinkled Surfaces Induced by Wood Mimetic Skins upon Drying: Effect of Mechanical Properties on Wrinkle Morphology. *Langmuir* **2016**, *32*, 12799–12804. [CrossRef] [PubMed]
22. Thakur, V.K.; Thakur, M.K. Recent Advances in Graft Copolymerization and Applications of Chitosan: A Review. *ACS Sustain. Chem. Eng.* **2014**, *2*, 2637–2652. [CrossRef]
23. Tian, M.; Tan, H.; Li, H.; You, C. Molecular weight dependence of structure and properties of chitosan oligomers. *Rsc. Adv.* **2015**, *5*, 69445–69452. [CrossRef]
24. Li, M.G.; Joung, D.H.; Hughes, B.; Waldman, S.D.; Kozinski, J.A.; Hwang, D.K. Wrinkling Non-Spherical Particles and Its Application in Cell Attachment Promotion. *Sci. Rep.* **2016**, *6*. [CrossRef] [PubMed]
25. Izumi, R.; Komada, S.; Ochi, K.; Karasawa, L.; Osaki, T.; Murahata, Y.; Tsuka, T.; Imagawa, T.; Itoh, N.; Okamoto, Y.; et al. Favorable effects of superficially deacetylated chitin nanofibrils on the wound healing process. *Carbohydr. Polym.* **2015**, *123*, 461–467. [CrossRef] [PubMed]
26. Minami, S.; Okamoto, Y.; Saimoto, H.; Shigemasa, Y. Effects of Chitin and Its Derivatives on Wound-Healing Acceleration Mechanisms. *J. Chitin Chitosan Sci.* **2014**, *2*, 163–178. [CrossRef]
27. Azuma, K.; Ifuku, S.; Osaki, T.; Okamoto, Y.; Minami, S. Preparation and biomedical applications of chitin and chitosan nanofibers. *J. Biomed. Nanotechnol.* **2014**, *10*, 2891–2920. [CrossRef] [PubMed]
28. Beanes, S.R.; Dang, C.; Soo, C.; Ting, K. Skin repair and scar formation: The central role of TGF-beta. *Exp. Rev. Mol. Med.* **2003**, *5*, 1–22. [CrossRef]
29. Hutter, J.L.; Bechhoefer, J. Calibration of Atomic-Force Microscope Tips. *Rev. Sci. Instrum.* **1993**, *64*, 1868–1873. [CrossRef]
30. Butt, H.J.; Cappella, B.; Kappl, M. Force measurements with the atomic force microscope: Technique, interpretation and applications. *Surf. Sci. Rep.* **2005**, *59*, 1–152. [CrossRef]
31. Rehfeldt, F.; Brown, A.E.X.; Raab, M.; Cai, S.S.; Zajac, A.L.; Zemel, A.; Discher, D.E. Hyaluronic acid matrices show matrix stiffness in 2D and 3D dictates cytoskeletal order and myosin-II phosphorylation within stem cells. *Integr. Biol.* **2012**, *4*, 422–430. [CrossRef] [PubMed]
32. Ogawa, Y.; Azuma, K.; Izawa, H.; Morimoto, M.; Ochi, K.; Osaki, T.; Ito, N.; Okamoto, Y.; Saimoto, H.; Ifuku, S. Preparation and biocompatibility of a chitin nanofiber/gelatin composite film. *Int. J. Biol. Macromol.* **2017**, *104 Pt B*, 1882–1889. [CrossRef] [PubMed]